Aerodynamic Analysis of Helicopter Rotor Blades in Heavy Rain Condition

Tung Wan , Hsiang-Chun Kuan
Department of Aerospace Engineering, Tamkang University, Taiwan, ROC

Abstract

Recently the greenhouse and global warming effects are becoming more and more severe, that partially explains why rainfall rates are keep breaking record continuously in all parts of the world. Currently helicopter has widespread utilization by air rescue unit in Taiwan during disaster situation under extreme weather situations. For this reason thus the understanding and improvement of helicopters under heavy rain condition is the main theme of this research. With our understanding of heavy rain physics, CFD tool has first being developed and successfully tested on the standard helicopter blade. Once the heavy rain droplets are added, it is observed that rainfall indeed will induce some detrimental effects on the main rotor blade's performance. Therefore, it is highly recommended that every helicopter pilot should be aware of this information gained in this work and has extensive training in some heavy rain situations.

Keywords：Helicopter, Rotor blades, Heavy rain, Aerodynamic analysis, MRF

1. Introduction

The greenhouse and global warming effects are becoming more and more detrimental to human being. Especially in Taiwan, last year a very serious flood occurs in southern Taiwan. Therefore, we need to pay more attention to this phenomenon and its influence on the helicopter aerodynamic performance during rescue mission. However, flight tests are extremely expensive and time-consuming tasks. Therefore we are often found palliatives solutions rather than optimized solutions. In addition, it is hard to complicate the configuration of helicopter main rotor blades and transmission mechanism, and there are many difficulties to model the real atmospheric environment such as gust winds and heavy rain. Nowadays, the advancement of technology and numerical simulation gave us a different simulation scenario environment. CFD is the branches of fluid mechanics that uses numerical methods and algorithms to solve and analyze highly nonlinear problems that involve fluid flows. Computers are used to perform the calculations required to simulate the interaction of liquids and gases with surfaces defined by proper boundary conditions. Latest ongoing research, however, may yield software that improves the accuracy and speed of complex simulation scenarios such as helicopter transonic or turbulent flows involving heavy rain physics. Initial validation of such software is often performed using a wind tunnel with the final validation coming in flight test, but at present we will limit ourselves with the numerical verification.

The field of helicopter aerodynamics is a vast one, which includes a number of current research problems and which are extremely important to us now. Accordingly, we have to pay attention to the most part on the nature of the wake by the rotor blades and the loads that the wake induces; the issue of turbulence and turbulence modeling in the computation of the rotor wake is leaved until heavy rain consideration. Helicopter performance depends largely on the thrust and lift that main rotor blades provide; therefore, the accurate modeling of composite helicopter rotor blades is an important element. Blade design and analysis is essential item in helicopter research and development process. Generally there are four primary elements of helicopter blades aerodynamic performance consideration, namely, chord length, twist angle, airfoil type or shape, and blade aspect ratio. After a timely research on the existing documentation, we decide to choose

NACA0012 airfoil with aspect ratio of 6 and taper ratio of 1 as our benchmark case to test and verify experiment data, and use existing CFD tool, and we have implemented it successfully in simulating fixed wing aerodynamic performance with heavy rain effects. Now it's time to further our investigation to the more complicated helicopter rotor blade's performance.

2. Research Background

2.1 Literature Review

As regarding the rotor blades tip vortex flow in the literature, a great deal of existing vortex flow paper use NACA0012 airfoil to construct the basic blade geometry. Although this airfoil is a simple and old fashioned model, but most research on vortex-blade interactive or aerodynamic analyses all employ it as the sample. In the early 80's, NASA F. X. Caradonna and C. Tung used experimental method to probe into rotor blade flow field [1]. The instrument as show in Figure 1, the profile as show in Figure 2:

They use instrument measure condition to investigate tip vortex strength and divination surface lift, building suspension performance situation method by rotor blade. Their study involves simultaneous blade pressure measurements and tip vortex surveys. Measurements were made for a wide range of tip Mach numbers including the transonic flow. The measured tip vortex strength and geometry permit effective blade loading predictions when used as input to a prescribed wake lifting surface code. It is also shown that with proper inflow and boundary layer modeling, the supercritical flow regime may be accurately predicted. So about the NASA paper it main four conclusions. First, vortex measurement technique seems to be quite effective for two bladed rotors. Second, at low rotor speeds, an untwisted, un-tapered, double-blade rotor produces tip vortices which can closely resemble a classical Rankine vortex. Except for the lowest pitch settings, this vortex strength closely approaches the blade bound circulation. At higher tip speeds, the inner vortex structure is outstanding; however, the strength is unaltered. Third, it is not possible to predict the blade span-wise load without accurate vortex location and strength data; so the blade vortex location and strength in span-wise are most important. Forth, the transonic flow model technology is only use nonlinear aerodynamic theory.

Agarwal etc.[2] used aerodynamic loads on a multi-bladed helicopter rotor in hovering flight are calculated to solving the 3-D Euler equations in a rotating coordinate system on body-conforming curvilinear grids around the blades. Euler equations are recast in the absolute flow variables so that the absolute flow in the far field is uniform but the relative flow is non-uniform. Equations are solved for the absolute flow variables employing Jameson's finite-volume explicit Runge-Kutta time-stepping scheme. Rotor-wake effects are modeled in the form of a correction applied to the geometric angle of attack along the blades. This correction is obtained by computing the local induced downwash with a free-wake analysis program. The calculations are performed on a CRAY/MP-48 supercomputer for a model helicopter rotor in hover at collective pitch angles. The results compared with experimental data. They find 3-D Euler equation can solve developed transonic flow on rotor blades of a helicopter in hover. The computational code is robust, efficient, and accurate. Computing power currently available on the machines, wake modeling is still needed for accurate calculation of aerodynamic loads.

In the paper by G. R. Srinivasan and W. J. McCroskey, their unsteady, thin-layer Navier-Stokes equations written in rotor coordinates are solved using a flux-split approximately factored, implicit, numerical algorithm to calculate the quasi-steady flow field of a hovering rotor blade [3]. And test cases chosen correspond to the experimental model hover test conditions of Caradonna and Tung. Induced wake effects in the lifting calculations were accounted as a correction to the geometric angle of attack. But the numerical results compare very well with the experimental data for both lifting and non-lifting cases. Alternate methods were explored to calculate the hovering rotor flow field as a steady-state flow field on a fixed isolated blade, keeping the same circulation distribution as that of the hovering blade. Investigate two different

type vortex flows and wing interact problem, and use Navier-Stokes equations to calculate the zero lift and lift rotor flow field in subcritical and supercritical flows. Of the two options considered, the variable free stream Mach number case gave almost identical pressure distributions as that of rotor at both subcritical and supercritical flow conditions. The variable twist option, on the other hand, gave similar results only under subcritical flow conditions; the supercritical flow condition was dominated by stronger transonic shocks even in the tip region. Under conditions where the fixed blade flow field closely agreed with that of the hovering blade, the influence of the centrifugal forces can be felt to the overall flow field properties.

S.H. Wang of NCKU [4] has studied the flow field for a two-bladed rotor having the NACA0012 airfoil section in hover, and the computed results are compared with those in the related NASA Caradonna and Tung's report to evaluate the present solution procedure. Their near-field Euler solver uses a solution-adaptive grid scheme to improve the resolution of the acoustic signal. The error indicator is computed from the flow field solution and determines the regions for mesh coarsening and refinement. Computed results for high-speed impulsive noise compare favorably with experimental data for three different hovering rotor cases. Good agreements are obtained between the numerical results and the experiment. About above-mentioned research literature mostly helicopter model were used NACA 0012 airfoil and NASA F. X. Caradonna and C. Tung's experiment data to test and verify, so it is nature that we use the same model to analyze and validate our simulation.

According to literature research, the UH-1H helicopter rotor blades also use NACA0012 airfoil. The UH-1H began to roll off the manufacturing line in 1967 in the US and remained in production for 20 years, with many UH-1Ds upgraded to UH-1H standard. Currently it is the most popular used helicopter in Taiwan, operated by ROC's Army and National Air Rescue Corps. This helicopter and its rotor blades will be the focus of this research. The helicopter profile is shown in Figure 3:

2.2 Heavy Rain Physics

Within the torrential classification a 2000-mm/h rain will be characterized as very heavy, 1500-mm/h rain as heavy, a 1000-mm/h rain as severe, a 500-mm/h as moderate, and a 100-mm/h rain as light. Rain can affect a fixed wing airplane in several ways [5-8]:

i. Rain droplets striking the airplane impart a downward momentum.
ii. A thin water film results from the rain that increase the airplane mass.
iii. Roughness of an airfoil in rain is caused by droplet waviness to a film on the airfoil and fuselage. Drag will increase from 5 to 10% for a 100mm/h rain to more than 15 to 25% for a 2000mm/h rain rate. In addition, lift decreases of 10% for a 100mm/h rain to more than 30% for a 2000mm/h rain.
iv. Most importantly, stall angle of attack for a roughened (wet) airfoil is from 2 to 6 deg less than that for a clean airfoil.

We will use the Discrete Phase Model (DPM) to modeling the rain. The Lagrangian discrete phase model follows the Euler-Lagrange approach. The fluid phase is treated as a continuum by solving the time-averaged Navier-Stokes equations, while the dispersed phase is solved by tracking a large number of particles, bubbles, or droplets through the calculated flow field. The dispersed phase can exchange momentum, mass, and energy with the fluid phase.

The above discussion on the heavy rain physics are entirely about a 2-D fixed wing aircraft during take-off or landing phases, and recently it has been justified and extended to other types of aircraft wing [9-12]. To our best knowledge, this heavy rain phenomenon has never been investigated for the helicopter rotor blade, either numerically or empirically; and is the focal point of this proposed research project. It is felt that some different and more complex mechanism of helicopter rain physical process will be found.

3. Numerical Modeling

To understand the model and the choice of our tool are quite essential to our simulation. Certain experimental cases were

chosen as test cases to validate the pressure coefficient. The experiments were conducted by NASA F. X. Caradonna and C. Tung [1] to provide data to be used in the validation of future rotor performance codes. Blade pressure measurements were made for a two-bladed rotor over a wide range of tip Mach numbers from the incompressible to transonic flow regimes. The experiments blades were NACA 0012 airfoils with no twist or taper and a half degree of precone. Each blade had a radius of 3.75 ft (1.143 m) and an aspect ratio of 6. The root cutout was approximately equal to one chord. Both validation cases presented here use a rotor with 0° of collective pitch, with the first rotating at 1500 rpm, which corresponds to a tip Mach number of 0.52.The computational model of the rotor blades used in cases was same as the NASA report. The dimensions of the blades were set exactly equal to the dimensions of the blades used in the experiment (Figure 1). The blades airfoil shape is choosing for NACA0012 profile which is used in NASA benchmark experiments. The mean chord line is 0.16933 m. It were untwisted and un-tapered, has an aspect ratio of 6. The geometry model shape is shown in Figure 7 and Figure 8.

To create geometry and the generation of grids are the first steps in the CFD analysis. For this reason in this research, we use GAMBIT software which can achieve the task of creating geometry and generating grids. Hence, due to the simple geometry of our rotor blade, we first use the unstructured type of grid which is adopted for the mesh system. Unstructured grid is a tessellation part of the Euclidean plane or Euclidean space by simple shapes, such as triangles or tetrahedrals, in an irregular pattern. Unlike structured grids, unstructured grids require a list of the connectivity which specifies the way a given set of vertices make up individual elements. Ruppert's algorithm or Bowyer's scheme is often used to convert an irregularly shaped polygon into an unstructured grid of triangles [13]. So, unstructured grids create is easy and have fine quality than structured grids in complex shapes.

The far meshes we constructed are shown in Figure 9 and Figure 10. The detailed near mesh of the rotor blade and blade surface are shown below in Figure 11 and Figure 12. The main body is using cubic type grids to compute in the outer region, and the side of outer boundary is 20m in length. Rotational mesh is of cylinder type and near the rotor blade, with a disk radius of 3m and a 2m height. So far, we have gained some experience in the grid generation software such as Gambit, Gridgen, ICEM, and Harpoon. It is felt that for 3-D complicated and even rotating configurations such as ours, among them Gambit and Gridgen seem most useful and easy to implement. The obstacle of negative volume region for a 3-D multi-block structured grid system has just being overcome.

The initial governing equations of this flow problem are the Euler equations. The mass conservation equation, or continuity equation, can be written as follows:

$$\frac{\partial \rho}{\partial t} + \nabla \square (\rho \vec{v}) = S_m \tag{1}$$

Equation (1) is the general form of the mass conservation equation and is valid for incompressible as well as compressible flows. The source is the mass added to the continuous phase from the dispersed second S_m phase. For 2-D axisymmetric geometries, the continuity equation is given by

$$\frac{\partial \rho}{\partial t} + \frac{\partial}{\partial x}(\rho v_x) + \frac{\partial}{\partial r}(\rho v_r) + \frac{\rho v_r}{r} = S_m \tag{2}$$

where x is the axial coordinate, r is the radial coordinate, v_x is the axial velocity, and v_r is the radial velocity. How to construct effective grids and choosing fine discretization method are the major concerns in CFD. For this benchmark test case, it is felt that a set of Euler equations is sufficient, although the unsteadiness has to come into play. But once we get to the real heavy rain simulation, the above governing equations have to become the standard Navier-Stokes type.

Advances in CFD in last two decades have provided the basis for further insight into the dynamics of multiphase flows. Currently there are two approaches for the numerical calculation of multiphase flows: the Euler-Lagrange approach and the Euler-Euler approach. Heavy rain could be

simplified as homogeneous phenomenon. The Euler-Euler approach is much suitable than Euler-Lagrange approach. There are several parameters should be considered, such as LWC (Liquid Water Content), rain rate, rain fall velocity and volume fraction. LWC (g/m^3) has relationship with rain rate (mm/hr) [8]:

$$LWC = 0.054R^{0.84} \tag{3}$$

Subsequently, we should determine the rain droplet speed when impacting the airfoil, thus the terminal velocity of each rain droplet is necessary for our investigation. The meaning of rain droplet terminal velocity is that during free fall, the falling droplet is eventually maintaining an equilibrium speed and is not accelerating. The reason is that frictional drag force due to air and the gravity force are in equilibrium. The terminal velocity of a raindrop is a function of droplet size and altitude, and it has been established by Marlowitz [14] as

$$V_T(m/s) = 9.58\{1 - \exp[-(\frac{D_d(mm)^{1.147}}{1.77})]\} \tag{4}$$

The relationship between the droplet size and the terminal velocity is showing in Figure 13, revealing the upper bound of the terminal velocity due to the equilibrium of gravity, drag, and surface tension.

To consider the helicopter rotating blade working under the heavy rain, the single phase governing equations turn into two phases. The continuity equation for phase q is

$$\frac{\partial(\alpha_q \rho_q)}{\partial t} + \nabla \cdot (\alpha_q \rho_q \vec{v}_q) = \sum_{p=1}^{n} (\dot{m}_{pq} - \dot{m}_{qp}) \tag{5}$$

where α_q and $\vec{v}_q$ is the volume fraction and velocity of phase q and $\dot{m}_{pq}$ characterizes the mass transfer from the pth to qth phase, and $\dot{m}_{qp}$ characterizes the mass transfer from qth to pth phase. The conservation equation of momentum for phase q yields

$$\frac{\partial}{\partial t}(\alpha_q \rho_q \vec{v}_q) + \nabla \cdot (\alpha_q \rho_q \vec{v}_q \vec{v}_q) = -\alpha_q \nabla p + \nabla \cdot \bar{\bar{\tau}}_q + \sum_{p=1}^{n} (\vec{R}_{pq} + \dot{m}_{pq} \vec{v}_{pq} - \dot{m}_{qp} \vec{v}_{qp}) + S_q \tag{6}$$

where $\bar{\bar{\tau}}_q$ is the qth phase stress-strain tensor, $\vec{R}_{pq}$ is an interaction force between phases, and $\vec{v}_{pq}$ is the inter-phase velocity. In here, the temperature change is too small to be considered, so that the energy equations could be ignored. The governing equations now can be simplified to have two sets of conservation of mass and momentum. However, in order to closely resemble the real atmospheric situation, the viscosity effect of the fluid needs to be considered. In this study, the k-ε turbulence model is chosen and tested with best results.

In FLUENT, the flow features associated with multiple rotating parts can be analyzed using the multiple-rotating reference frame (MRF) capability. This model is powerful in that multiple rotating frames can be included in a single domain. The resulting flow field is representative of a snapshot of the transient flow field in which the rotating parts are moving. However, in many cases the interface can be chosen in such a way that the flow field at this location is independent of the orientation of the moving parts.

Taken from case description appearing in the existing manual, this particular case has a rotor radius of 3m; it contains fifty blades, and rotates at 1500 rpm. The blade rotation is simulated by the MRF model in FLUENT. This steady-state representation of the moving cylinder uses a rotating frame of reference for the blade region, and a stationary frame of reference for the inlet is cube. Information is continually passed between these two regions across a cylindrical interface as the solution progresses. Experience gained from this test is useful for our helicopter problem solving.

In FLUENT, using the coupled algorithm enables full pressure-velocity coupling, hence it is referred to as the pressure-based coupled algorithm. In our model, the boundary condition velocity inlet is set to approach to zero is 0.00001m/s, the rotor speed is 157.079rad/s. For incompressible flow, the density is set to pressure-based. Control solver is set to be SIMPLE, discretization pressure and momentums are set as Standard and Second Order Upwind respectively.

4、Results and Discussion

After the unceasing test and simulation, the best result model grid we achievable is 2.21 million, and the blade surface grid is about 0.30 million. The resulting pressure coefficient values are very close to the NASA experimental data, as shown in the Figure 14. Here pressure coefficient is an important and fundamental parameter, because it can let us know the variation at different blade location. But for $C_{P_{old}}$, it cannot include the rotation parameter($r\omega$) automatically. We have to modify $C_{P_{old}}$ into $C_{P_{new}}$, as shows in the following equation:

$$C_{P,old} = \frac{P - P_\infty}{\frac{1}{2}\rho v_\infty^2} \tag{7}$$

$$C_{P,new} = \frac{P - P_\infty}{\frac{1}{2}\rho[v_\infty^2 + (r\omega)^2]} \tag{8}$$

So

$$C_{P,new} = \frac{C_{P,old} v_\infty^2}{[v_\infty^2 + (r\omega)^2]} \tag{9}$$

Eq. (9) now is in accordance with the existing helicopter blade's experimental and numerical simulation data. The upper and lower surface blade data line are shown below in Figure 14. Current numerical simulations are the inviscid unsteady 2.21 million grid line; and it's quite encouraging.

Compare our results with the existing test data and other numerical values; it seems that current work is indeed success. This also proved the validity of the software Fluent if properly implemented. Finally, Figure 15 is showing the upper and lower surface pressure coefficient comparison of clean and rain conditions of 39g/m^3 liquid water content at y/R=0.50, 0.80, 0.96 stations. It is clearly shown the major difference made by the heavy rain situation considered here, and representing more than 3 percent degradation in the helicopter total lift performance. This experience gained by our research group in the grid construction and the selection of solver scheme in last 3 years will be the building block of our future intensive simulation.

5、Conclusions

The simulation of heavy rain effects on 2-D airfoil in our research group was started with modification of incoming rain flow density and angle of attack, with the addition of an artificial water film on the airfoil upper surface. Later this approach has been replaced by a two-phase flow simulation built in Fluent's DPM mechanism, and applied to traditional 2-D airfoil, 2-D high-lift devices, low speed UAV's wing, and even a Blended-Wing-Body (BWB) aircraft. Compared with existing experimental data, our results seem reasonable and encouraging, and clearly showing the importance of heavy rain contribution in helicopter blade performance.

With the success of our calculation in the benchmark rotor blade case, and the experience gained by our research teams in heavy rain simulation via the two-phase flow approach, we are cautious but quite confident that future works in this heavy rain simulation will go quite smoothly. As before, our heavy rain cases will consist of liquid water content other than 39g/m^3. Considering the loss of 3 lives in the rescue mission in August 2009, it is believed that the findings of this work will be helpful to the civilian helicopter rescue missions under forthcoming severe weathers.

References

[1] Caradonna, F. X., and Tung, C., "Experimental and Analytical Studies of a Model Helicopter Rotor in Hover," NASA TM-81232, 1981.

[2] Agarwal, R. K., "Euler Calculations for Flowfield of a Helicopter Rotor in Hover," *Journal of Aircraft*, Vol.24, No.4, April 1987, pp231-238.

[3] Srinivasan, G. R., and McCroskey, W. J., "Navier-Stokes Calculations of Hovering Rotor Flowfields," *Journal of Aircraft*, Vol.25, No.10, 1988, pp865-874.

[4] Wang, S. H., "On the rotor blade flow and acoustics simulation by adaptive finite volume method", NCKU MS Thesis, 2005.

[5] "NASA Will Study Heavy Rain Effect on Wing Aerodynamics", Aviation

Week & Space Technology, Feb. 13, 1989.
[6] Thompson, B. E., and J. Jang, "Aerodynamic Efficiency of Wings in Rain", *Journal of Aircraft*, Vol. 33, No. 6, 1996.
[7] Valentine, James, R., "Airfoil Performance in Heavy Rain," *Transportation Research Record*, No. 1428, Jan. 1994, pp. 26-35.
[8] Thompson, B. E., J. Jang, and J. L. Dion, "Wing Performance in Moderate Rain," *Journal of Aircraft*, Vol. 32, No. 5, Sept.-Oct. 1995, pp.1034-1039.
[9] Wan, T., and S.W. Wu, "Aerodynamic Analysis under the Influence of Heavy Rain," *Journal of Aeronautics, Astronautics and Aviation*, Vol. 41, No. 4, September 2009.
[10] Wan, T., and H. Yang, "Aerodynamic Performance Investigation of a Modern Blended- Wing-Body Aircraft under the Influence of Heavy Rain Condition," Proceedings of the 8th Asian Computational Fluid Dynamics Conference, Hong Kong, January 10-14, 2010.
[11] Wan, T., and S.P. Pan, "Aerodynamic Efficiency Study under the Influence of Heavy Rain via a Two-phase Flow Approach," Proceedings of 24th International Congress of Aeronautical Sciences (ICAS), Nice, France, September 19-24, 2010.
[12] Tsai, P.C., C.H. Lin, and T. Wan, "A Two-phase Flow Approach for UAV Aerodynamic Study under Heavy Rain," Proceedings of 2009 AASRC/CSCA Joint Conference, Nankong, December 12, 2009.
[13] Wan, T. and Yip, F., "The Study of 3-D Unstructured Grid Generation with Bowyer Scheme," *Transactions of Aeronautical and Astronautical Society of Republic of China*, Vol. 29, No. 1, January-February, 1997, pp. 55-63.
[14] Markowitz, A. M., "Raindrop Size Distribution Expression", *Journal of Applied Meteorology*, Vol. 15, 1976, pp. 1029-1031.
[15] Bezos, G. M., Dunham, R. E. Jr., Gentry, G. L. Jr., and Melson, W. E. Jr., "Wind Tunnel Aerodynamic Characteristics of a Transport-Type Airfoil in a Simulated Heavy Rain Environment", NASA Technical Paper 3184, 1992.
[16] Lawson, R. P., Angus, L. J., and Heymsfield, A. J., "Cloud Particle Measurements in Thunderstorm Anvils and Possible Weather Threat to Aviation," *Journal of Aircraft*, Vol. 35, No. 1, January-February 1998, pp. 203-212.
[17] Wan, T., and Wu, S. W., "Aerodynamic Analysis under Influence of Heavy Rain," Proceedings of 24th International Congress of Aeronautical Sciences (ICAS), Yokohama, Japan, September 14-19, 2004.
[18] Algermissen, G., and Wagner, S., "Computation of Helicopter BVI Noise by Coupling Free-Wake, Euler and Kirchhoff Method," AIAA-98-2238, 1998.
[19] Kang, H.J., and Kwon, O.J., "Unstructured Mesh Navier-Stokes Calculations of the Flow Field of a Helicopter Rotor in Hover," *Journal of the American Helicopter Society*, Vol. 47, No. 2, April 2002.
[20] Adriano, G., "CFD Analysis and Design of a Low-Twist, Hovering Rotor Equipped with Trailing-Edge Flaps," University of Glasgow Thesis, 2007.
[21] Mineck, R., E., and Gorton, S., A., "Steady and Periodic Pressure Measurements on a Generic Helicopter Fuselage Model in the Presence of a Rotor." NASA TM-2000-210286, 2000.

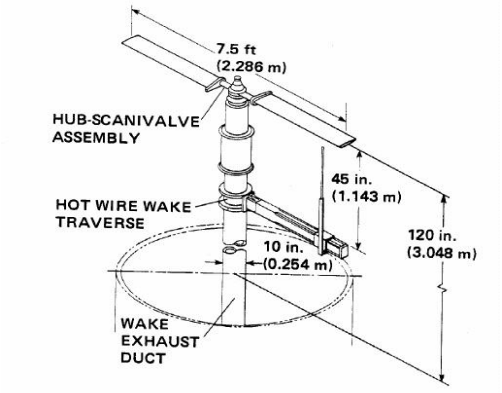

Figure 1 The NASA model and experiments set-up. [1]

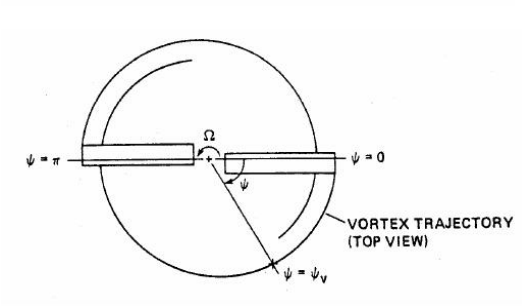

Figure 2 The NASA model profile. [1]

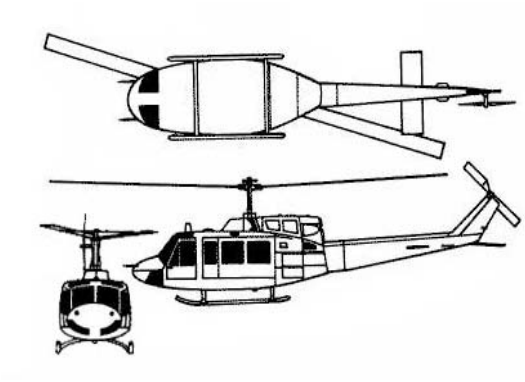

Figure 3 The UH-1H helicopter profile

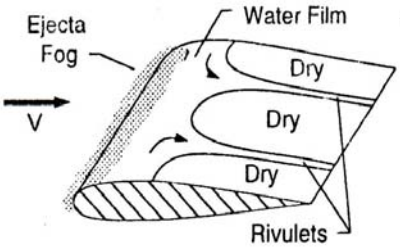

Figure 4 Sketch of water behavior on top of wing surface[8]

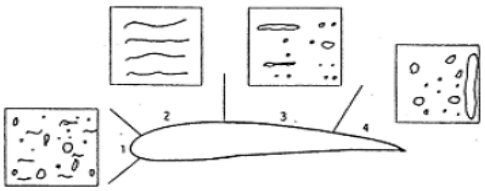

Figure 5 Characteristics of four surface water flow regions: 1.droplet-impact region; 2. film-convection region; 3. rivulet-formation region; 4. droplet-convection region. [9]

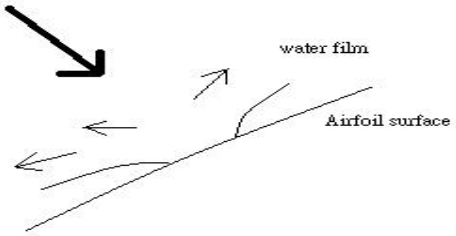

Figure 6 The film cratering from droplet impact. [9]

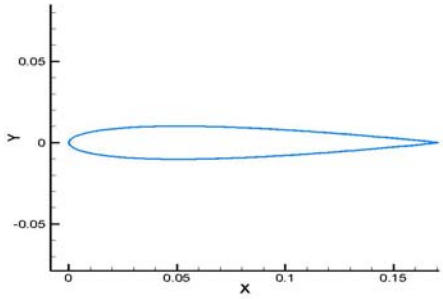

Figure 7 The NACA 0012 airfoil section profile

Figure 8 The rotor blades profile

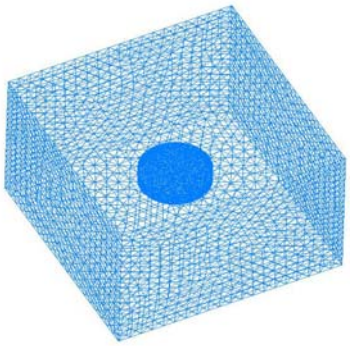

Figure 9 Far mesh of the rotor blades

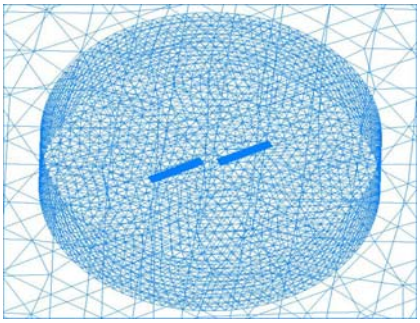

Figure 10 Rotation mesh of the rotor blades

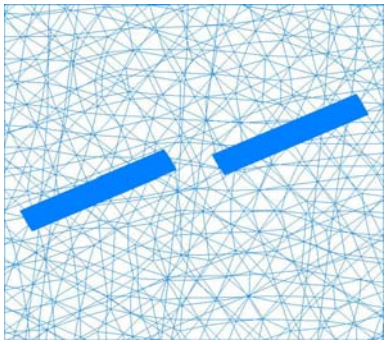

Figure 11 Near mesh of the rotor blades

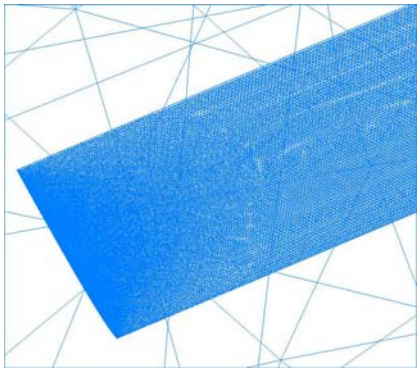

Figure 12 Near mesh of the blade surface

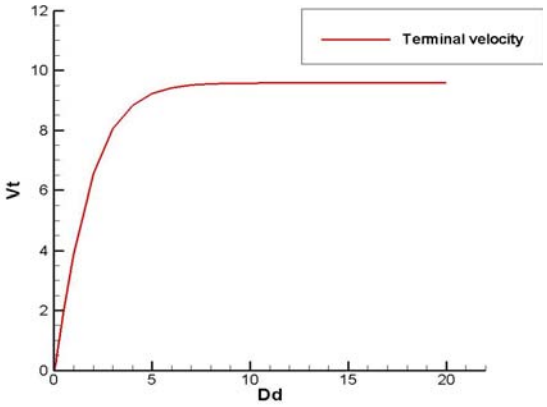

Figure 13 The relationship between droplet size and terminal velocity

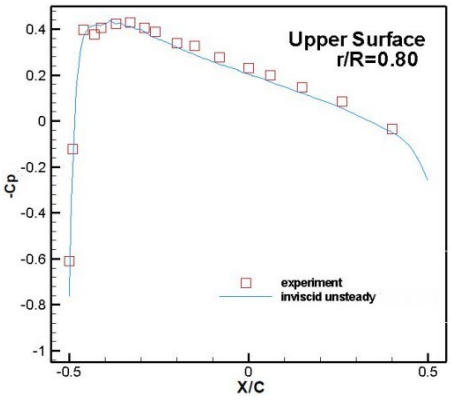

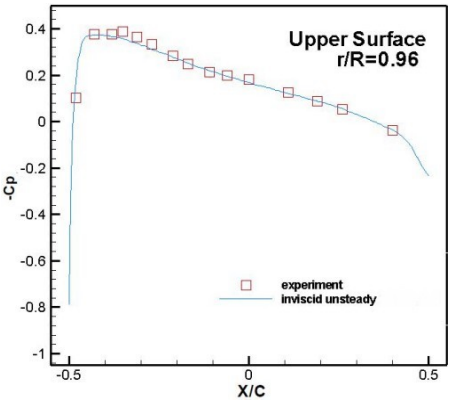

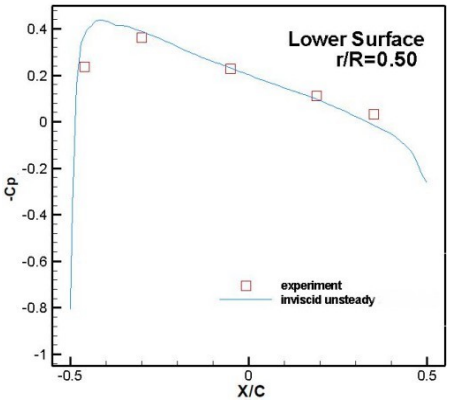

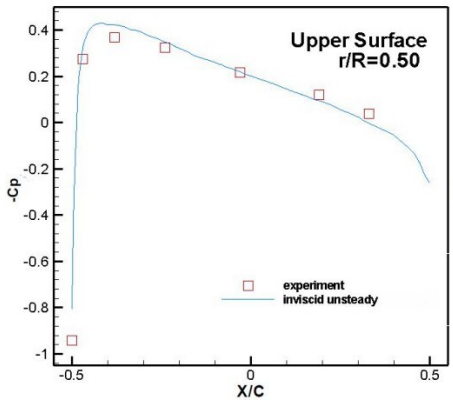

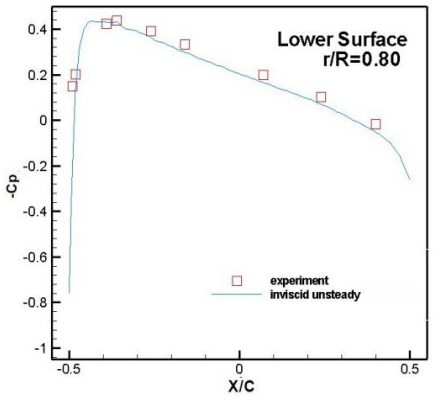

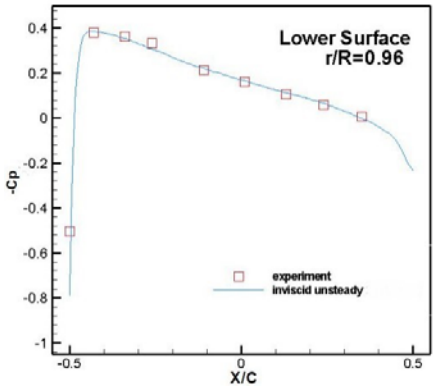

Figure 14 The upper and lower surface pressure coefficient compare with NASA experimental and numerical result [4] at y/R=0.50, 0.80, 0.96

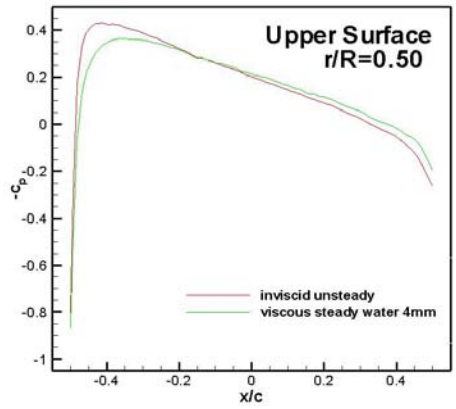

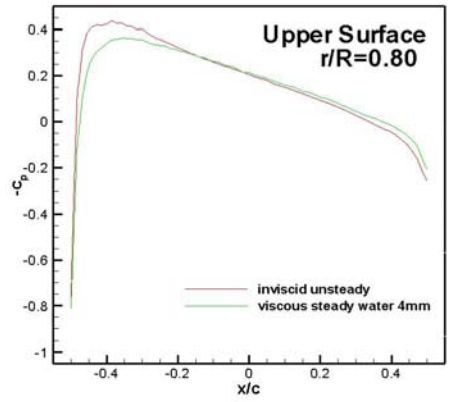

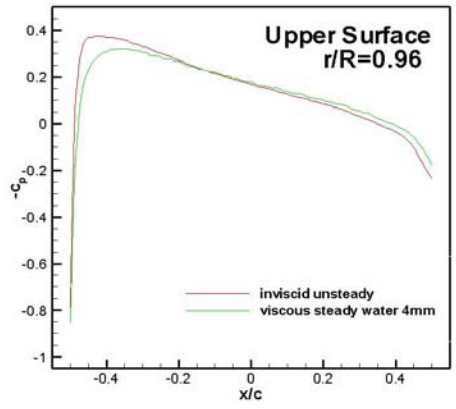

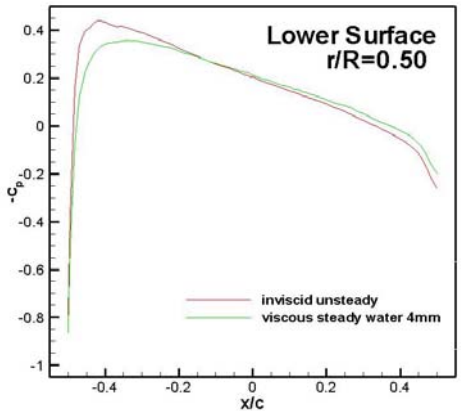

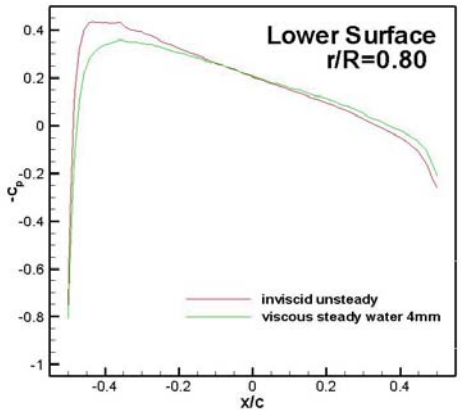

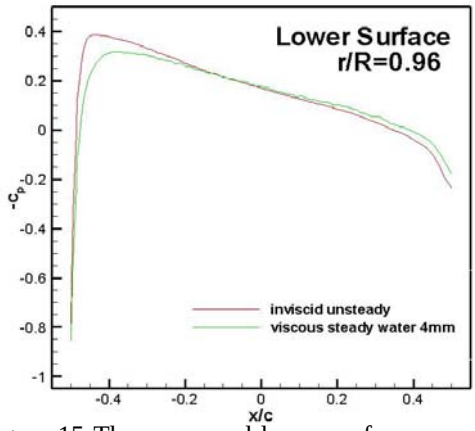

Figure 15 The upper and lower surface pressure coefficient comparison of clean and rain conditions at y/R=0.50, 0.80, 0.96